ACS APPLIED MATERIALS & INTERFACES

www.acsami.org

Research Article

Shape-Switchable Liquid-Crystal Polymer Actuators with Light-Induced Shape Memory Effect

Jinlei Wang, Feng Pan, Xiaojun Liu, Lang Qin,* and Yanlei Yu

Cite This: ACS Appl. Mater. Interfaces 2025, 17, 48815−48823

Read Online

ACCESS | Metrics & More | Article Recommendations | Supporting Information

ABSTRACT: The initial shape of a soft actuator plays a vital role in its functional performance as it dictates the internal stress distribution and deformation pathway during the actuation process. Photodeformable liquid-crystal polymers (LCPs) have demonstrated significant potential in soft actuators due to their fast, localized, precise, and reversible deformation under light irradiation. However, the initial shape of LCP actuators is generally nonswitchable once fabricated, limiting them to a single deformation mode and monofunctionality. Herein, we present a strategy for fabricating shape-switchable LCP actuators by integrating an athermal light-induced shape memory effect (SME) into photodeformable LCP systems. The reversible photodimerization of coumarins introduces an additional crosslinking network that regulates the mobility of molecular chains, enabling LCPs to exhibit a light-induced SME for shape-switching. Moreover, the photothermal effect of disperse red 1 acrylate induces mesogen alignment changes under 470 nm light irradiation, allowing for the independent actuation of each switched shape. Leveraging this unique shape-switching mechanism, we fabricated a soft actuator capable of transforming among multiple motion modes, including rolling, crawling, and gripping, for the first time. This study establishes a novel design paradigm for developing multimorphology and multifunctional soft actuators, advancing the complexity and versatility of LCP-based intelligent systems.

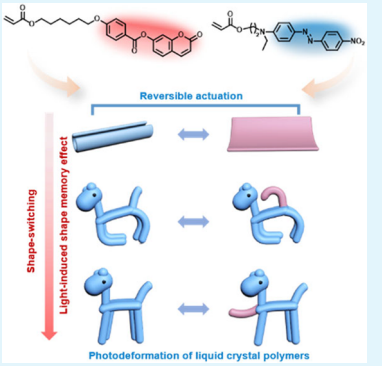

KEYWORDS: *liquid-crystal polymers, photodeformation, soft actuators, photo-crosslinking, shape memory effect*

1. INTRODUCTION

Soft actuators, fabricated from soft materials, have emerged as a highly promising technology in fields such as soft electronics, biomedical devices, soft robotics, and surgical applications owing to their stimuli-responsive and programmable shape-changing capability.[1−4] Liquid-crystal polymers (LCPs) have demonstrated significant potential in soft actuators due to their programmable and reversible deformation in response to external stimuli, such as heat, electric fields, light, and magnetic fields.[5−13] Among the diverse external stimuli, light stands out owing to its advantages of clean energy usage, wireless manipulation, and spatially localized control.[14−20] Recently, doping photothermal agents such as gold nanorods,[21] graphene oxide,[22] organic dyes,[23] and polydopamine[24] into LCP matrices has emerged as a promising strategy for designing photodeformable LCPs due to their fast response and excellent long-term stability. Upon irradiation at a specific wavelength, light is converted into thermal energy, locally heating the LCP beyond its nematic-to-isotropic phase transition temperature (T_{NI}), thereby inducing reversible photodeformation. By regulating the mesogen alignment within LCPs, various photodeformation modes including bending,[25,26] twisting,[27] and contracting[28] have been realized under light irradiation. Additionally, the initial shape of the LCP actuator is a key factor influencing its functional performance, as it dictates the internal stress distribution and deformation pathway during the actuation process.[29−31] Even with identical molecular alignment patterns, variations in the shape lead to distinct actuation behaviors and functional outputs. Typically, a uniaxially aligned LCP film doped with photothermal agents exhibits light-induced reversible contraction owing to mesogen alignment changes.[32] Moreover, by twisting the ends of a uniaxially aligned LCP film clockwise and then gluing them in a head-to-head manner, a ring-shaped actuator is fabricated. This actuator exhibits uniform in-plane contraction when irradiated with 808 nm light at the twist regions, followed by a continuous rotation.[33] Researchers have also fabricated a light-induced snapping actuator by assembling a fin-array structure onto a uniaxially aligned film using an in situ crosslinking method, followed by bonding the two sides of the film with acrylate adhesive. Upon light irradiation, graphene within the LCP converts light into thermal energy, inducing local contraction due to changes in the mesogen alignment. Once this contraction releases the

Received: June 26, 2025
Revised: August 6, 2025
Accepted: August 8, 2025
Published: August 12, 2025

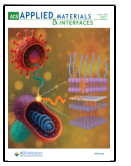

https://doi.org/10.1021/acsami.5c12533
ACS Appl. Mater. Interfaces 2025, 17, 48815−48823

mechanical constraint imposed by the adhesive, the stored elastic energy is instantaneously released, resulting in a rapid jumping behavior.[34] However, the initial shape of LCP actuators is generally nonswitchable once fabricated, limiting them to a single deformation mode and monofunctionality. Developing advanced shape-switchable LCP actuators is particularly attractive as it enables the realization of multifunctionality in actuation systems by changing the shape of the soft actuator.

Utilizing the shape memory effect (SME), the initial shape of the polymer can be readily switched into various temporary shapes, such as three-dimensional (3D) cranes, 3D flowers, and origami/kirigami structures, which recover upon exposure to external stimuli.[35−40] The essence of the shape-switching in a typical thermally induced shape memory process originates from the activation of molecular chain motion by heating the polymer above its shape memory transition temperature, such as the glass transition temperature (T_g) or melting temperature (T_m), thereby enabling shape programming under external force. Subsequent cooling freezes the molecular chains, storing the strain energy and fixing the programmed shape. Upon reheating, the stored strain energy is released, allowing the temporary shape to recover as the molecular chains unfreeze again.[41−43] Incorporating SME into the LCP system holds great potential for fabricating shape-switchable actuators. However, when thermally induced SME is integrated into the LCP system, the shape programming and recovery process may raise the temperature above the phase transition temperature of the LCP. This process leads to the simultaneous triggering of strain energy release and mesogen alignment changes, which presents a challenge for achieving well-controlled shape-switching and subsequent reversible actuation. A plausible strategy to address these problems is to introduce an athermal light-induced SME into the photodeformable LCP system since the athermal shape-switching process minimally affects the ordered mesogen alignment. Incorporating photoreversible covalent bonds into polymers offers an effective approach to endow the material with the athermal light-induced SME.[44−48] The reversible photodimerization of photoresponsive moieties introduces dynamic and reversible chemical crosslinks, enabling precise control over molecular chain motion without thermal interference, thereby preserving the ordered mesogen alignment and maintaining the reversible photodeformation capability of the LCP system after shape switching.

Herein, a crosslinked LCP (CLCP) containing the photothermal agent disperse red 1 acrylate (DR1A) and the reversible photodimerization moiety coumarin is synthesized, which demonstrates a reversible photodeformation based on the photothermal effect and the athermal light-induced SME. The CLCP exhibits a shape-switching behavior driven by the athermal light-induced SME, as the reversible photodimerization of coumarin moieties forms additional chemical crosslinking points that regulate molecular chain mobility under alternating 312 and 254 nm light irradiation. Each switched shape retains its ability to undergo reversible actuation upon 470 nm irradiation, because the molecular chain motion minimally affects the ordered mesogen alignment during the shape-switching process. Moreover, a splay orientation is selected to enhance the bending deformation due to asymmetric expansion and contraction on the two opposite surfaces of the CLCP film. Utilizing the unique shape-switching capability, we fabricate an actuator capable of transforming among distinct motion modes including rolling, crawling, and gripping.

2. EXPERIMENTAL SECTION

2.1. Materials. Liquid-crystal (LC) monomers RM82 and RM23 were obtained from JvSheng Chemical (Hubei) Co. Photoinitiator 819, 7-hydroxycoumarin, disperse red 1-D3(DR1-D3), acryloyl chloride, 4-(6-prop-2-enoyloxyhexoxy)benzoic acid, triethylamine, 4-dimethylaminopyridine, and 1-(3-(dimethylamino)propyl)-3-ethylcarbodiimide hydrochloride (EDC) were bought from Adamas (Shanghai, China). Polyimide (PI) prepolymers for the alignment layer were purchased from Kelide Optoelectronic Materials Co. Ltd.

2.2. Measurements. ^{1}H NMR spectra of the monomers were recorded on a Bruker DMX500 NMR spectrometer using tetramethylsilane as the internal standard and $CDCl_3$ as the solvent. The textures of the LC mixture were evaluated with a polarized optical microscope (POM, Leika, DM2500p) equipped with a hot stage (Linkam THMS600). The thermodynamic properties of CLCP were determined by differential scanning calorimetry (DSC, TA, Q2000) at a heating and cooling rate of 10 °C min^{-1}. The UV−vis spectra of CLCP were measured by using a UV−vis spectrometer (PerkinElmer Lambda 650, 200−800 nm) at a resolution of 2 nm. Images and videos of the deformation behaviors were obtained with a super-resolution digital microscope (Keyence, VHX-1000C). 312 and 254 nm UV light was generated by a Zhongke microenergy CME-M500 light source. 470 nm visible light was generated by a CCS HLV-24GR-3W.

2.3. Synthesis of DR1A. DR1-D3 (6.29 g, 20 mmol) was added into a 500 mL flask and dissolved in 80 mL of dichloromethane. After complete dissolution, the flask was placed in an ice-water bath, and then acryloyl chloride (5.43 g, 60 mmol) was added dropwise into the mixture and stirred for 5 h. The crude product was filtrated to remove the precipitates and purified by column chromatography with silica gel using dichloromethane. Finally, red solid DR1A (1.54 g, yield 21%) is obtained. The ^{1}H NMR results are shown in Figure S1.

2.4. Synthesis of Coumarin-Containing Acrylate Monomer (CAM). 4-(6-(Acryloyloxy)hexoxy)benzoic acid (2.93 g, 1 mmol) and 4-dimethylaminopyridine (1.22 g, 10 mmol) were added into a 250 mL flask and dissolved in 50 mL of dichloromethane. After complete dissolution, the flask was placed in an ice-water bath, and then 7-hydroxycoumarin (1.62 g, 1 mmol) and EDC (5.74 g, 30 mmol) were added dropwise into the mixture and stirred for 30 min. Then, the system was transferred to room temperature and reacted for 20 h. The crude product was filtrated to remove the precipitates and purified by column chromatography with silica gel using dichloromethane. Finally, the white solid CAM (2.75 g, yield 43%) is obtained. The ^{1}H NMR results are shown in Figure S2.

2.5. Synthesis of the Crosslinked LCP CLCP-CAM. The homogeneous LC mixtures (taking CLCP with 20% CAM content as an example), consisting of 43.3 mol % RM82, 36.4 mol % RM23, 2 mol % DR1A, 17.3 mol % CAM, and 1 mol % photoinitiator 819, were filled into homemade LC cells by capillary force on a heating stage at 70 °C. The LC mixtures formed were splay-aligned and fixed by photopolymerization upon exposure to UV light (5 mW cm^{-2}, 10 min) to obtain red pristine CLCP-CAM20. The polymerization temperatures of CLCP with different CAM contents are provided in Table S2.

2.6. Fabrication of the LC Cell. First, the glass substrates (5 cm × 6 cm) were cleaned by sonication in ethanol for 3.5 h and treated with oxygen plasma for 300 s to activate the glass surfaces. Second, the bottom glass substrates of the LC cells were spin-coated (3000 rpm, 40 s) with PI prepolymers (KPI-9811) that were subsequently cured by two-step imidization at 80 °C for 1 h and 240 °C for 2 h. The PI-coated glass substrates were then mechanically rubbed with a rayon velvet cloth by a rubbing machine (HOLMARC, HO-IAD-BTR-02), generating the alignment layer parallel to the rubbing direction. The upper glass substrates of the LC cells were spin-coated (3000 rpm, 40 s) with PI prepolymers (KPI-3000) that were subsequently cured by two-step imidization at 80 °C for 1 h and 240 °C for 2 h, generating the alignment layer homeotropic to the rubbing direction. Lastly, the 25 μm spacers were stuck on either side of the bottom glass substrates, which were bound with the upper glass substrates to fabricate the splay-aligned LC cells by UV-curable adhesive.

https://doi.org/10.1021/acsami.5c12533
ACS Appl. Mater. Interfaces 2025, 17, 48815−48823

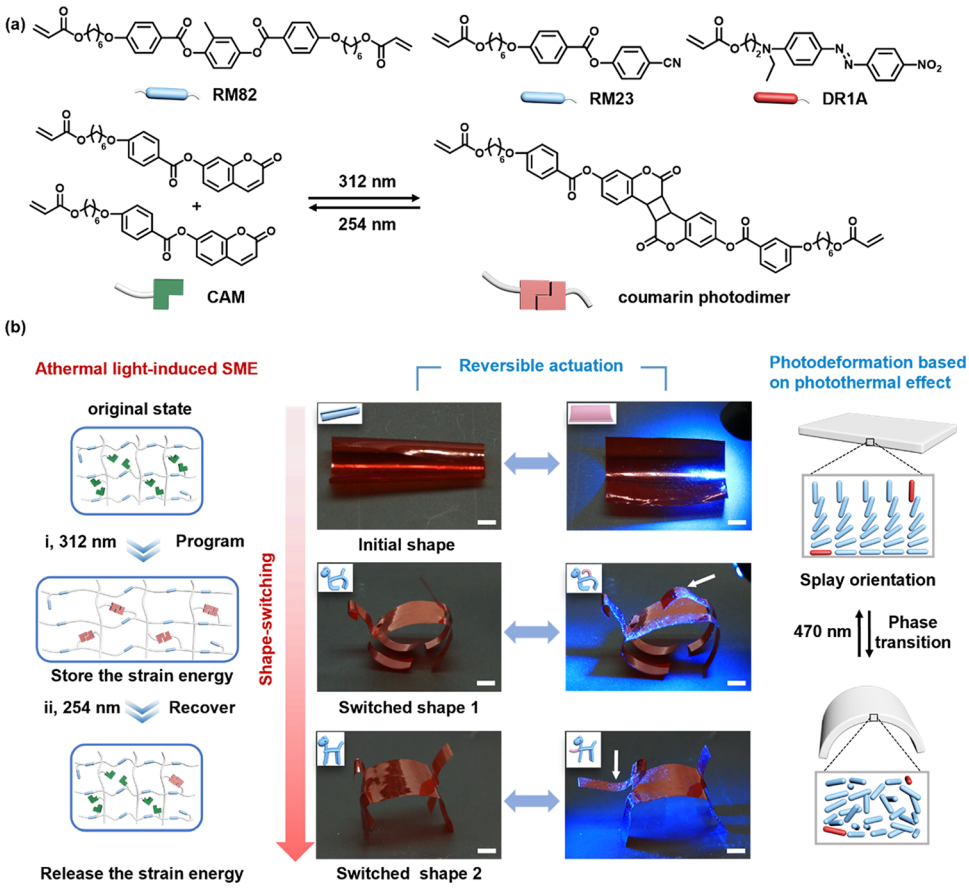

Figure 1. (a) Chemical structures of the LC monomers RM82 and RM23, the photothermal agent DR1A, the CAM, and the coumarin-based dimer. (b) Schematic illustration of the shape-switching process and the reversible photodeformation of each switched shape. The associated changes in the molecular-scale aggregation structure, including mesogen alignment and polymer chain configuration, are also depicted. Step (i): the initial shape of the CLCP-CAM20 film was programmed into a lying-down pony by applying external force and then fixed under 312 nm UV light irradiation. Step (ii): upon irradiation of specific regions with 254 nm UV light, the programmed shape transformed into another stereoscopic shape due to the release of strain energy driven by the photo-de-crosslinking of the CLCP. Scale bar: 2 mm.

2.7. Shape-Switching Process of the CLCP-CAM. The initial shape of CLCP-CAM is programmed by applying an external force, followed by irradiation with 312 nm UV light (5 mW cm^{-2}) for 1.5 h. This process induces the coumarin groups to form additional chemical crosslinks, which store strain energy and fix the temporary shape. The switched shape 1 is obtained after removal of the external force. Upon irradiating with 254 nm (2 mW cm^{-2}) UV light for 0.5 h, the switched shape 2 is obtained owing to the release of strain energy triggered by the photocleavage of coumarin groups.

3. RESULTS AND DISCUSSION

The key point of our strategy lies in introducing the athermal light-induced SME to achieve shape-switching without disrupting the ordered mesogen alignment, thereby ensuring that each switched shape retains its ability to undergo reversible actuation. Therefore, two photosensitive monomers with distinct driven wavelengths, CAM and DR1A, were introduced into the LCP system to achieve independent control over the molecular chain motion and mesogen alignment changes. The reversible photodimerization of CAM, driven by 312 and 254 nm UV light, introduces additional reversible chemical crosslinks, which can be harnessed to regulate the molecular chain motion for strain energy storage and release. Meanwhile, the photothermal effect of DR1A, driven by 400−600 nm visible light, is responsible for controlling the mesogen alignment change (Figure 1a). The detailed synthetic routes and characterizations of CAM and DR1A are depicted in the Section 2 and Figures S1 and S2. The polymeric films were fabricated using cells with one rubbed planar polyimide and one homeotropic polyimide-coated plate, which are glued together using 25 μm spacers and filled by the LC mixture of RM82, RM23, CAM, DR1A, and photoinitiator 819. After photopolymerizing the mixture in its nematic phase under 365 nm UV light irradiation (5 mW cm^{-2}) for 10 min, the CLCP-CAM films with a thickness of 25 μm were obtained.

Employing CLCP-CAM20 as the construction material, shape-switching of the LCP and reversible actuation of each switched shape is demonstrated in Figure 1b. Initially, the CLCP-CAM film bent in the direction of the homeotropic polymer side due to the anisotropic internal stress generated during photopolymerization.[49] In addition, the initial bending degree of the CLCP-CAM was connected with anisotropic thermal expansion, which increased with the temperature difference between the pre- and postpolymerization states.[50] The curved sheet was programmed into a stereoscopic pony in a lying-down posture by applying an external force and then irradiated with 312 nm UV light to trigger the [2 + 2] cycloaddition of the coumarin groups. This reaction formed additional chemical cross links that stored strain energy and fixed the shape (step (i)). Subsequently, the strain energy was released after irradiation with 254 nm UV light owing to the photocleavage of coumarin, causing the lying-down pony to

https://doi.org/10.1021/acsami.5c12533
ACS Appl. Mater. Interfaces 2025, 17, 48815−48823

gradually stand up (step (ii)). Importantly, each state of the pony exhibited local and reversible actuation upon 470 nm visible light irradiation, owing to the order−disorder phase transition of CLCP-CAM induced by the photothermal effect. The actuation includes dynamic deformation of the tail and a biomimetic reaching behavior of the foreleg extending forward (Movies S1 and S2).

To investigate the effect of CAM content on the aggregation structure of the CLCP, which influences the photodeformation and shape-switching behavior, a series of CLCP-CAMx were synthesized, where x denotes the mole fraction of CAM in the monomer mixture. First, the composition of the LC mixture used to prepare CLCP-CAM is presented in Table S1, with a fixed molar ratio of RM82 to RM23 chosen for optimal performance.[51] After the photopolymerization, the CLCP-CAM film is obtained, and the basic properties of CLCP-CAM are summarized in Table 1. The liquid crystalline properties of the mixture remain largely unaffected by the increased CAM content, which is attributed to the structural compatibility between CAM and the host mesogens RM82 and RM23. The T_{NI} of the LC mixtures, measured by POM, decreased from 86 to 58 °C with an increase in the CAM content from 5 to 50% (Figure S3). The decrease is due to the lower clearing point of the CAM, which gradually becomes the main component of the LC mixture, leading to a synergistic reduction in T_{NI}. Additionally, the isotropization transition of CLCP-CAM was not observed in the differential scanning calorimetry (DSC) curves (Figure S4) owing to the motion of LC molecules being tightly confined by the polymer network after polymerization. The T_g of various CLCP-CAMx was around 50 °C, indicating that the crosslinked network remained the dominant factor restricting chain mobility, resulting in little change in the T_g. Furthermore, splay orientation, in which the LC director gradually transitions from planar alignment at one surface to homeotropic alignment at the opposite surface across the film thickness, is employed to enhance the bending deformation due to the asymmetric expansion and contraction on the two sides of the CLCP film.

Table 1. Material Properties of LC Mixtures and the Corresponding CLCP with Varying Molar Ratios of CAM

sample	CAM (mol %)	DR1A (mol %)	phase transition temperature (T_{NI}/°C)	glass transition temperature (T_g/°C)
CLCP-CAM5	5	2	86	49
CLCP-CAM10	9	2	74	50
CLCP-CAM20	17.3	2	71	50
CLCP-CAM30	23.8	2	66	49
CLCP-CAM40	29.4	2	60	50
CLCP-CAM50	34.2	2	58	50

The splay-aligned CLCP-CAMx films bend toward the planar-aligned side consistently under 470 nm light, regardless of the illuminated surface. To investigate this deformation behavior in detail, the CLCP-CAM40 film (3 × 12 × 0.025 mm) was selected as a representative example. The film was suspended and fixed at one end between two glass slides and then irradiated with 470 nm light. As shown in Figure 2a, the film bent away from the light source when the homeotropic side was irradiated, which is attributed to surface expansion induced by mesogen alignment change. In contrast, irradiation of the planar

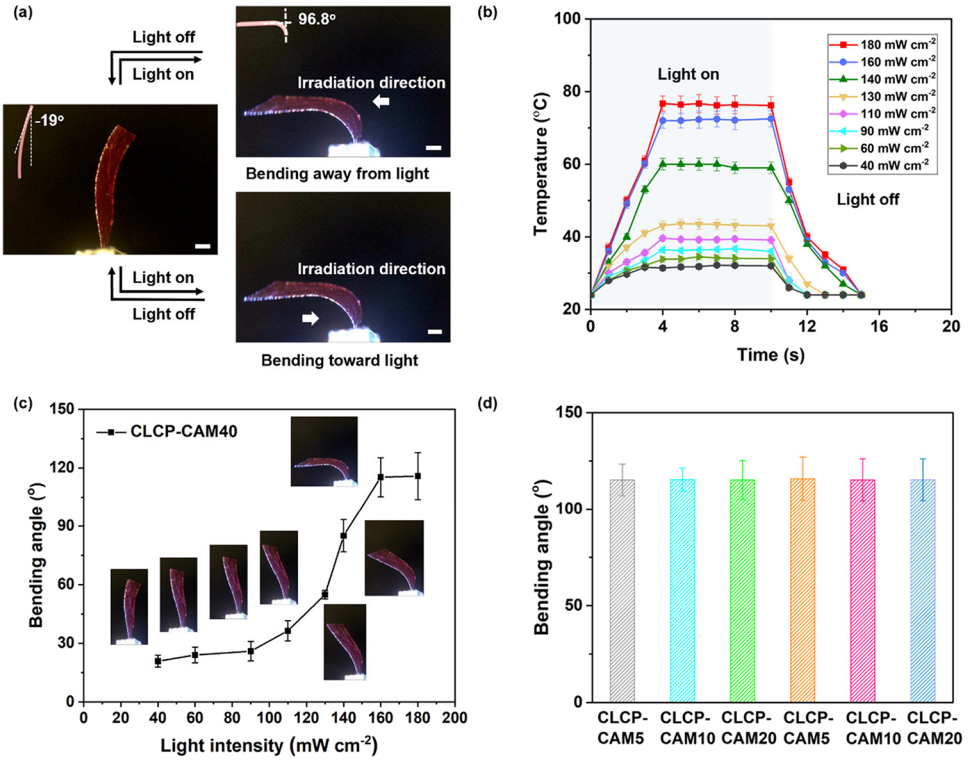

Figure 2. (a) Images of the reversible bending of the splay-aligned film CLCP-CAM40 in different directions under 470 nm light (180 mW cm^{-2}) irradiation; scale bar: 2 mm. (b) Real-time surface temperature profiles of the CLCP-CAM40 film irradiated by 470 nm light of various intensities. (c) Light-intensity-dependent bending angle of CLCP-CAM40. (d) Maximum bending angle of CLCP-CAMx when irradiating with 180 mW cm^{-2} 470 nm light.

https://doi.org/10.1021/acsami.5c12533
ACS Appl. Mater. Interfaces 2025, 17, 48815−48823

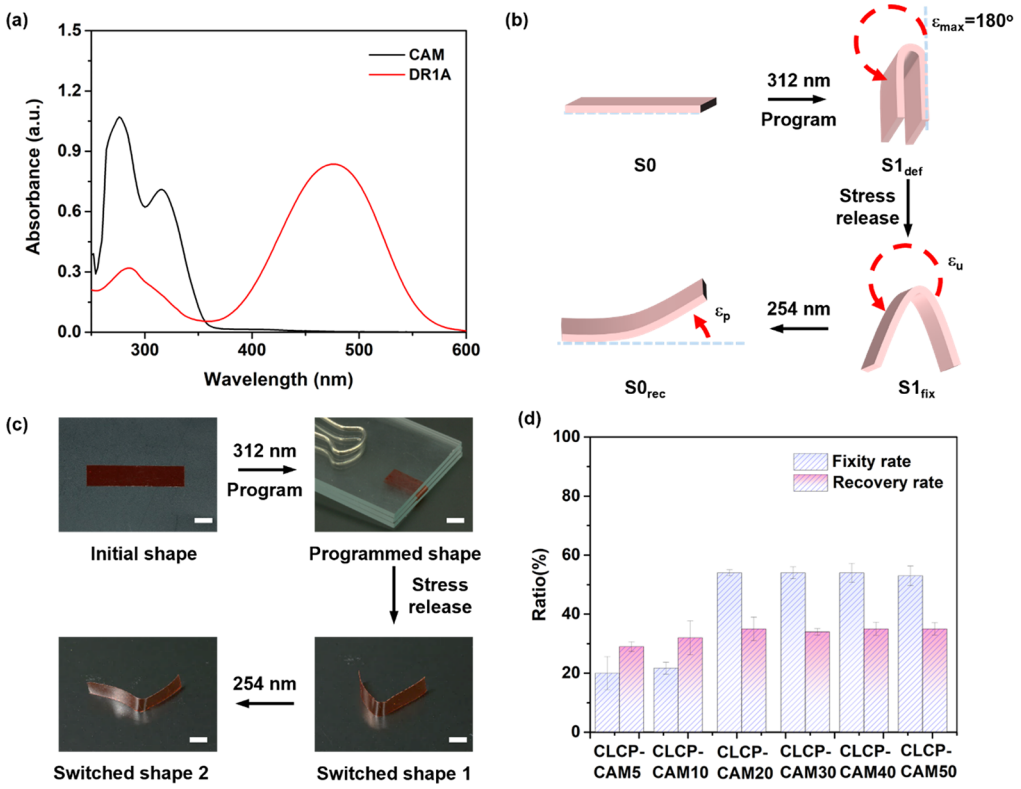

Figure 3. (a) UV−vis adsorption spectra of CAM and DR1A. (b) Programming and recovery protocols for light-directed shape-switching behavior. The shape fixity and recovery ratio are calculated by the bending angle of the film; ε_{max} is the folding angle programmed by external force; ε_u is the fixation angle after stress release; and ε_p is the recovered angle after the shape recovery process. The shape fixity ratio is calculated by the equation $R_f = \varepsilon_u/\varepsilon_{max}$; The shape recovery ratio is calculated by the equation $R_r = (\varepsilon_u - \varepsilon_p/\varepsilon_u)$. (c) Images of the CLCP-CAM40 strip sample (12 mm × 2 mm × 25 μm) at different states during the shape programming and recovery process; scale bar: 1.5 mm. (d) Light-triggered shape fixity and recovery ratio of CLCP-CAMx.

side resulted in surface contraction, causing bending toward the light source. The CLCP-CAM40 film exhibited a maximum bending angle of approximately 116° under a light intensity of 180 mW cm^{-2} and returned to its initial shape upon cessation of the light. Based on these observations, we further evaluated the illumination conditions required for large-scale deformation and examined the influence of the CAM content by measuring the photothermal effect and corresponding bending angles of the CLCP-CAMx films. Figure 2b−d illustrates the quantitative photothermal conversion efficiency of CLCP-CAM. The CLCP-CAM40 film exhibited a rapid photothermal response, with its temperature rising from 24.5 to 79.9 °C within 4 s as the light intensity increased to 180 mW cm^{-2} (Figure 2b). Although the bending angle reaches its maximum under 160 mW cm^{-2} light irradiation, further increasing the light intensity to 180 mW cm^{-2} leads to a continued rise in the surface temperature; yet only a minimal increase in bending angle is observed. This implies that the LCP undergoes a complete transition to the isotropic phase under 160 mW cm^{-2} light irradiation, and further heating results in only a negligible enhancement in deformation (Figure 2c). A marked increase in deformation amplitude was observed when the intensity exceeded 140 mW cm^{-2}, attributed to the temperature of the film approaching the T_g of the polymer (Figure S5), enhancing the molecular chain mobility that facilitated the alignment change of mesogens. The bending behavior of films with various CAM contents was further investigated in Figure 2d. All films exhibited excellent photodeformation behavior, with maximum bending angles of approximately 116° when the temperature of the film exceeded the T_{NI}, indicating that the CAM content in the CLCP had minimal impact on the deformation behavior. This is because the similar core structure of CAM ensured good compatibility with the LC mixture, maintaining its ability to align along the rubbing direction. Moreover, the film demonstrated stable light-induced bending during 30 cycles without obvious fatigue (Figure S6). The combination of excellent cycling performance, rapid response, and controllable deformation provided a solid foundation for constructing actuators with continuous motion.

The athermal light-induced SME of CLCP-CAMx was investigated in detail, serving as the foundation for the shape switching. First, to identify the wavelengths responsible for the reversible photodimerization of CAM, while distinguishing them from those that induce mesogen alignment changes, the UV−Vis absorption spectra of the two photoresponsive components were recorded. As shown in Figure 3a, CAM exhibited two absorption peaks within the 250−350 nm range, corresponding to the benzene ring absorption (250−350 nm) and the conjugated double bond of the coumarin moiety (300−350 nm). In contrast, the DR1A spectrum displayed a dominant absorption band in the range of 400−600 nm, attributed to the characteristic $\pi-\pi$ transitions of the azobenzene units. The clear spectral separation between CAM and DR1A enables independent control over the light-induced SME and the reversible photodeformation. Moreover, the reversible photodimerization and photocleavage reaction of CAM introduced an additional reversible chemical crosslink, which can be harnessed for regulating molecular chain motion to store and release strain energy. The characteristic absorbance peak at 320 nm, which is

https://doi.org/10.1021/acsami.5c12533
ACS Appl. Mater. Interfaces 2025, 17, 48815−48823

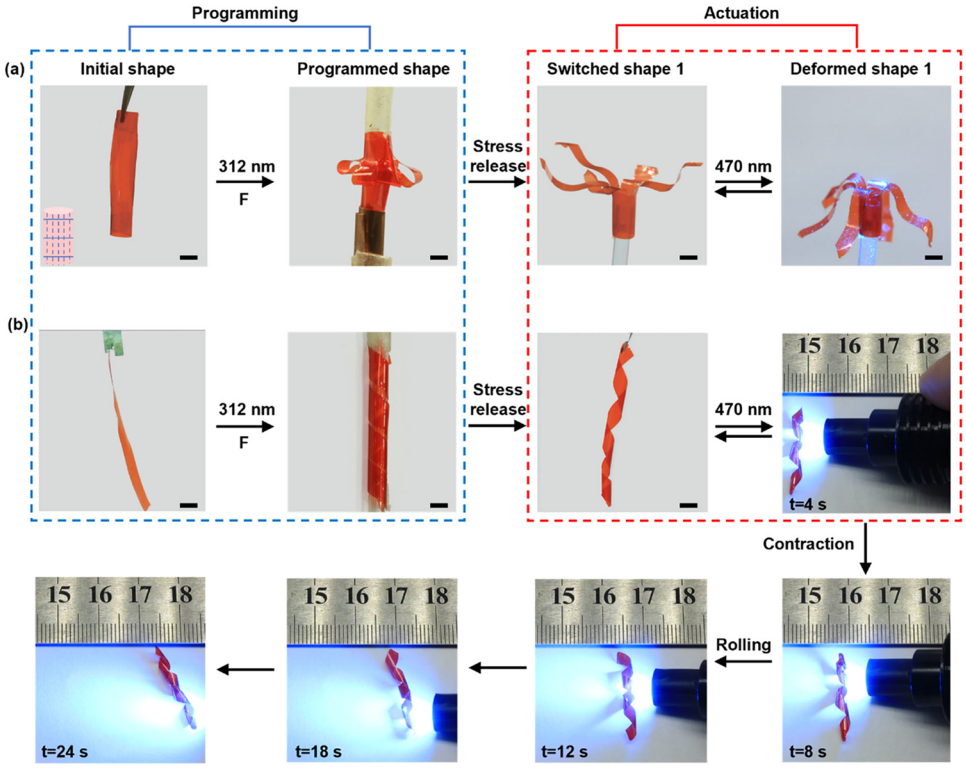

Figure 4. (a) Images showing the deployed shape of CLCP-CAM40 programmed by external force and fixed via photo-crosslinking under 312 nm irradiation, along with its local and reversible actuating behavior under 470 nm light irradiation at 180 mW cm^{-2}; scale bar: 2 mm. Solid lines indicate the folding creases, and dashed lines indicate the cutting seam. (b) Images showing the spiral shape of CLCP-CAM40 programmed by an external force and fixed via photo-crosslinking under 312 nm irradiation, and its continuous rolling behavior under 470 nm light irradiation. Scale bar: 4 mm.

ascribed to the double bond of the coumarin moiety, gradually decreases under 312 nm light irradiation, indicating dimerization to form a cyclobutane ring[35] (Figure S7a). Upon subsequent irradiation with 254 nm light, the absorbance peak gradually increased, indicating the photoscission reaction of the dimers (Figure S7b). In addition, the light intensity used to trigger the SME in our system is only 5 mW cm^{-2}. At this low intensity, no significant temperature increase is observed on the film surface, and thus, the alignment of the LC molecules remains unaffected, as shown in Figure S8.

Leveraging the reversible photo-crosslinking of CLCP-CAMx, the following shape-switching process was investigated. As shown in Figure 3c,d, a flat permanent strip (S0) obtained by tailoring the center of the film was programmed into a folded temporary shape ($S1_{def}$) by applying external force, followed by irradiation with 312 nm light for 1.5 h to induce the photo-crosslinking, thereby storing strain energy and fixing the shape. After removal of the external stress, switched shape 1 was obtained ($S1_{fix}$). Upon irradiation with 254 nm for 30 min, the temporary shape transformed into the switched shape 2 ($S0_{rec}$) due to the release strain energy triggered by the photo-de-crosslinking of the film. To evaluate the influence of the CAM content on the aggregation structure of CLCP that affects the shape-switching behavior, the light-induced shape fixity and recovery ratios were calculated based on the bending angle change of the strip during a shape memory cycle. As shown in Figure 3b, the light-induced shape fixity and recovery ratios increased with increasing CAM content, reaching a plateau at a concentration of 20%. The observed plateau can be attributed to two primary factors. First, although an increase in the coumarin content enhances the extent of photodimerization, the CLCP matrix already possesses a rigid crosslinked network. Therefore, the formation of additional crosslinks must overcome the mechanical constraints imposed by the pre-existing network. Due to this restriction, the efficiency of freezing the polymer chains during the new network formation is limited, and the suppression of elastic recovery from the original network is insufficient. As a result, the shape fixation ratio no longer increases with further CAM incorporation. Moreover, the photocleavage and photodimerization reactions of coumarin units exists in a dynamic equilibrium under 254 nm light irradiation.[52−54] As shown in the Figure S7b, the absorbance associated with the coumarin double bond gradually increases with increasing irradiation time at 254 nm, indicating the occurrence of photoscission of the dimers. However, the absorbance fails to fully return to its initial level, implying incomplete de-crosslinking. This limited reversibility of the crosslinked network likely contributes to the observed plateau in the shape recovery ratio. Furthermore, neither the shape fixation nor the recovery ratios improved with a higher light intensity because the photodimerization reaches an equilibrium state within 1.5 h of irradiation.[46] Notably, the partial shape recovery facilitates the attainment of multiple shapes during the shape-switching process, which contributes to enhancing the diversity of actuation functions in LCP-based intelligent systems. In addition, the effective number of shape-switching cycles achievable without significant performance degradation is at least three.

To validate the rationality of our design that changes in the mesogen alignment have a minimal impact on the mobility of molecular chains, the reversible photodeformation behavior of the switched shape 1 with stored strain energy was investigated.

https://doi.org/10.1021/acsami.5c12533
ACS Appl. Mater. Interfaces 2025, 17, 48815−48823

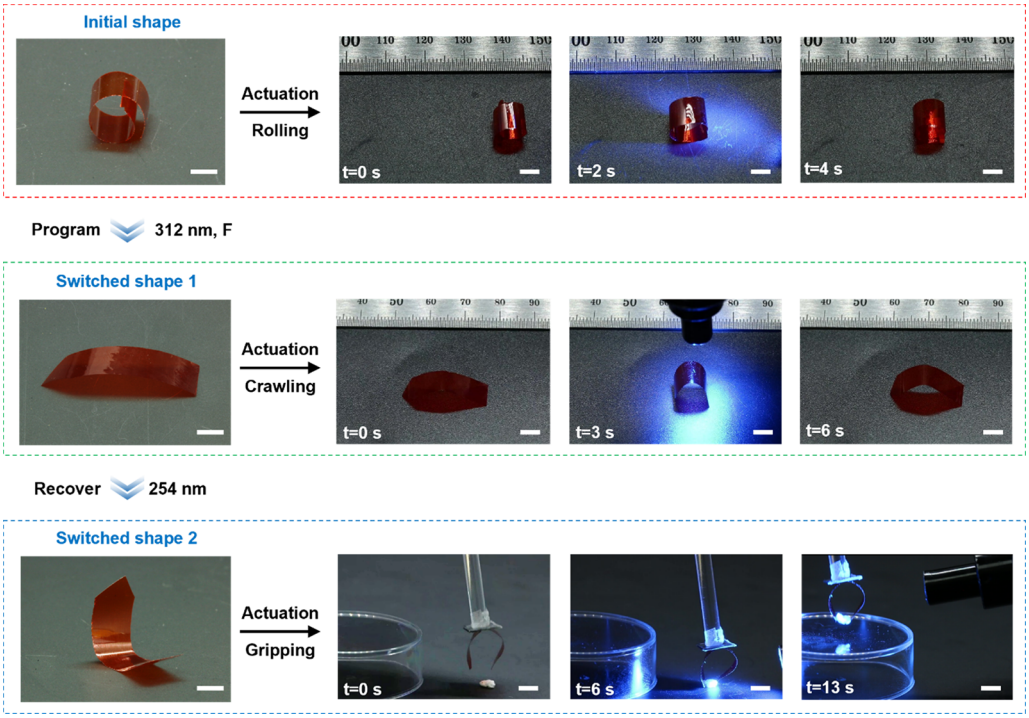

Figure 5. Images depicting the shape switching of CLCP-CAM20, driven by the reversible photo-crosslinking, and the reversible actuation of each shape followed by subsequent transformation of the actuation modes in the switched shape; scale bar: 4 mm.

As shown in Figure 4, two different switched shapes, obtained through different programming approaches, demonstrate independent reversible deformations upon 470 nm light irradiation. The initial origami shape is obtained by patterning cuts and bonding the two ends together. After cutting one end of the origami shape, the initial shape was programmed into a developed shape, and the shape was fixed by 312 nm light-induced photo-crosslinking. The spiral shape was fabricated by coiling a film with homeotropic alignment on the outer surface, followed by shape fixation via 312 nm light irradiation. Both the switched deployed shape and the spiral shape, with strain energy stored in their networks, underwent reversible deformation under 470 nm light irradiation without compromising the original configuration (Movies S3 and S4). Furthermore, a rolling actuator was constructed based on the spiral shape. As shown in Figure 4b, parts of the spiral shape bent away from the light due to the homotropic alignment of mesogens on the outer surface upon exposure to 470 nm visible light. The refined deformation shifted the barycenter of the shape, inducing the rolling behavior toward the light source. Subsequently, the light source was rapidly moved to the remaining part of the spiral shape, causing contraction and pushing the shape to roll toward the light source. The continuous motion of the rolling actuator illustrated that the temporary shape remained stable during actuation, implying that changes in mesogen alignment have little impact on the stored strain energy. Notably, the spiral shape with the planar-aligned side facing outward fails to achieve continuous rolling motion. As shown in Figure S9, the outer surface of the spiral structure bends toward the light source under 470 nm light irradiation due to mesogen alignment changes, leading to the unwinding of the spiral. Therefore, only when the homeotropic-aligned side is selected as the outer surface can the spiral structure exhibit rolling motion under light irradiation.

By harnessing the shape-switching behavior of CLCP-CAMx, we constructed an actuator capable of transforming among distinct motion modes, including rolling, crawling, and gripping, was constructed. As shown in Figure 5, an initial ring-shaped structure with a triangle tail-end was obtained by tailoring the curled portion of CLCP-CAM20, which exhibited a greater curvature due to the higher polymerization temperature of 71 °C. Upon 470 nm light irradiation, the mesogen alignment change on one side of the ring caused surface contraction, leading to the bending behavior toward the light source. Taking advantage of the large deformation, the barycenter of the ring tilted forward, resulting in a rolling motion (Movie S5). Subsequently, the permanent shape was programmed into a straight state and the temporary shape was fixed by 312 nm induced photochemical crosslinking. Upon 470 nm light irradiation, the film bent toward the light source until the bottom edges of both sides became vertical to the ground, leading to a caterpillar-like crawling motion due to the shifted barycenter (Movie S6). The photode-crosslinking of the temporary shape occurred when irradiated with 254 nm light, allowing the temporary shape to transform into a curved form. We then attached it to a glass rod using tape to create a simple ″gripper″ shape. Using this ″gripper″, the actuator successfully lifted a paper ball weighing 10 times its own weight upon 470 nm irradiation (Movie S7).

4. CONCLUSIONS

In conclusion, we developed a novel CLCP-CAMx system that integrates athermal light-induced SME and reversible photo-deformation by incorporating photo-crosslinking moieties coumarin and photothermal agents DR1A into the LCP matrix. The CLCP-CAMx exhibits a shape-switching behavior driven by the athermal light-induced SME, in which reversible photo-dimerization of coumarin moieties forms additional chemical crosslinks that regulate molecular chain mobility under

https://doi.org/10.1021/acsami.5c12533
ACS Appl. Mater. Interfaces 2025, 17, 48815−48823

alternating 312 and 254 nm light irradiation. Each switched shape retains its ability to undergo reversible actuation upon 470 nm irradiation as the molecular chain motion during the shape-switching process minimally affects the ordered mesogen alignment. Notably, partial shape recovery facilitates the attainment of multiple shapes during the shape-switching process, which contributes to enhancing the diversity of actuation functions in LCP-based intelligent systems. Utilizing the CLCP-CAM as a construction material, a soft actuator capable of transitioning among continuous motion modes, including rolling, crawling, and gripping, is fabricated. This study proposes a novel strategy for designing multifunctional soft actuators and highlights their promising potential in shape manipulation and task-specific functionalities, which are crucial for increasing the complexity of the deformation modes and the functional versatility of LCP actuators.

■ ASSOCIATED CONTENT

Supporting Information

The Supporting Information is available free of charge at https://pubs.acs.org/doi/10.1021/acsami.5c12533.

Additional information on the characterization of the monomers; POM images; DSC curves; infrared thermal images; UV−vis adsorption spectra; cycling performance and the actuation of spiral structure with planar-aligned side outward (PDF)

The reversible photodeformation of the tail of pony in a lying-down posture (MP4)

The reversible photodeformation of the foreleg of the pony (MP4)

The reversible photodeformation of the deploy-shaped actuator (MP4)

Photoinduced rolling behavior of the spiral-shaped actuator (MP4)

Photoinduced rolling behavior of the ring-shaped actuator (MP4)

Photoinduced crawling behavior of the actuator (MP4)

Photoinduced gripping behavior of the actuator (MP4)

■ AUTHOR INFORMATION

Corresponding Author

Lang Qin − *College of Smart Materials and Future Energy, State Key Laboratory of Molecular Engineering of Polymers, Fudan University, Shanghai 200438, P. R. China;* orcid.org/0000-0002-7439-225X; Email: qinlang@fudan.edu.cn

Authors

Jinlei Wang − *College of Smart Materials and Future Energy, State Key Laboratory of Molecular Engineering of Polymers, Fudan University, Shanghai 200438, P. R. China*

Feng Pan − *College of Smart Materials and Future Energy, State Key Laboratory of Molecular Engineering of Polymers, Fudan University, Shanghai 200438, P. R. China*

Xiaojun Liu − *College of Smart Materials and Future Energy, State Key Laboratory of Molecular Engineering of Polymers, Fudan University, Shanghai 200438, P. R. China*

Yanlei Yu − *College of Smart Materials and Future Energy, State Key Laboratory of Molecular Engineering of Polymers, Fudan University, Shanghai 200438, P. R. China;* orcid.org/0000-0002-4623-3331

Complete contact information is available at: https://pubs.acs.org/10.1021/acsami.5c12533

Author Contributions

This manuscript was written through contributions of all authors. All authors have given approval to the final version of the manuscript.

Notes

The authors declare no competing financial interest.

■ ACKNOWLEDGMENTS

This work was financially supported by the National Natural Science Foundation of China (52233001, 52173110), the Innovation Program of Shanghai Municipal Education Commission (2023ZKZD07), the Shanghai Rising-Star Program (22QA1401200), and the Foundation of the Shanghai Municipal Education Commission (24KXZNA05).

■ REFERENCES

(1) Rus, D.; Tolley, T. Design, Fabrication and Control of Soft Robots. *Nature* **2015**, *521*, 467−475.

(2) Li, M.; Pal, A.; Aghakhani, A.; Pena-Francesh, A.; Sitti, M. Soft Actuators for Real-Word Applications. *Nat. Rev. Mater.* **2022**, *7*, 235−249.

(3) Miriyev, A.; Stack, K.; Lipson, H. Hu. Soft Material for Soft Actuators. *Nat. Commun.* **2017**, *8*, 596.

(4) Chen, T.; Bilal, O.; Shea, K.; Daraio, C. Harnessing Bistability for Directional Propulsion of Soft, Untethered Robots. *Pro. Nat. Acad. Sci. USA* **2018**, *115*, 5698−5702.

(5) Lv, J.; Liu, Y.; Wei, J.; Chen, E.; Qin, L.; Yu, Y. Photocontrol of Fluid Slugs in Liquid Crystal Polymer Microactuators. *Nature* **2016**, *537*, 179−184.

(6) White, T.; Broer, D. Programmable and Adaptive Mechanics with Liquid Crystal Polymer Networks and Elastomers. *Nat. Mater.* **2015**, *14*, 1087−1098.

(7) Jin, B.; Chen, G.; Chen, Y.; Zhu, Z.; Weng, Y.; Zhao, Q.; Xie, T. Reprogramming Photoresponsive Liqudi Cyrstal Elastomer via Force-Directed Evaporation. *ACS Appl. Mater. Interfaces* **2024**, *16*, 16844−16852.

(8) Wu, Y.; Zhang, S.; Yang, Y.; Li, Z.; Wei, Y.; Ji, Y. Locally Controllable Magnetic Soft Actuators with Reprogrammable Contraction-Drived Motions. *Sci. Adv.* **2022**, *8*, No. eabo6021.

(9) Zhou, R.; Yang, B.; Zheng, N. Sequentially Autonomous Rolling of Liquid Crystalline Elastomers with Tunable Actuation Temperatures. *Acta Polym. Sin.* **2024**, *55*, 614−623.

(10) Lv, P.; Yang, X.; Bisoyi, H.; Zeng, H.; Zhang, X.; Chen, Y.; Xue, P.; Shi, S.; Priimagi, A.; Wang, L.; Feng, W.; Li, Q. Stimulus-Driven Liquid Metal and Liquid Crystal Network Actuators for Programmable Soft Robotics. *Mater. Horiz.* **2021**, *8*, 2475−2484.

(11) Pu, Y.; Zhang, X.; Liu, X.; Zhao, X.; Yang, Z.; Yu, Y. Multi-stimuli Responsive Bionic Actuators Constructed by Linear Liquid Crystal Polymers. *Transactions of Materials Research* **2025**, *1*, No. 100003.

(12) Xu, Y.; Huang, Y.; Wang, J.; Huang, S.; Yang, H.; Li, Q. Force-Trainable Liquid Crystal Elastomer Enabled by Mechanophore-Induced Radical Polymerization. *Angew. Chem., Int. Ed.* **2025**, *64*, No. e202423584.

(13) Hu, J.; Yu, Z.; Yang, Y.; Huang, J.; Liu, Z.; Huang, S.; Wang, M.; Yang, H. Graphene Nanoribbon Core Thermotropic Liquid Crystal with a Well-Defined Molecular Structure. *Angew. Chem., Int. Ed.* **2025**, *64*, No. e202501161.

(14) Pang, X.; Lv, J.; Zhu, C.; Qin, L.; Yu, Y. Photodeformable Azobenzene Containing Liquid Crystal Polymers and Soft Actuators. *Adv. Mater.* **2019**, *31*, No. 1904224.

(15) Gelebart, A.; Vantomme, G.; Meijer, E.; Broer, D. Mastering the Photothermal Effect in Liquid Crystal Networks: A General Approach for Self-sustained Mechanical Oscillators. *Adv. Mater.* **2017**, *29*, No. 1606712.

(16) Zhao, X.; Chen, Y.; Peng, B.; Wei, J.; Yu, Y. A Facile Strategy for the Development of Recyclable Multifunctional Liquid Crystal Polymers via Post-Polymerization Modification and Ring-Opening

Metathesis Polymerization. *Angew. Chem., Int. Ed.* **2023**, *62*, No. e202300699.
(17) Huang, X.; Pang, X.; Qin, L.; Yu, Y. Photodeformable Main-chain Crosslinked Liquid Crystal Polymer Fiber Actuators at Room Temperature. *Acta Polym. Sin.* **2022**, *53*, 1324−1331.
(18) Herbert, K.; Fowler, H.; McCracken, J.; Schlafmann, K.; Koch, J.; White, T. Synthesis and Alignment of Liquid Crystalline Elastomers. *Nat. Rev. Mater.* **2022**, *7*, 23−38.
(19) Hu, Z.; Fang, W.; Li, Q.; Feng, X.; Lv, J. Optocapillarity-Driven Assembly and Reconfiguration of Liquid Crystal Polymer Actuators. *Nat. Commun.* **2020**, *11*, 5780.
(20) Iamsaard, S.; Aßhoff, S.; Matt, B.; Kudernac, T.; Cornelissen, J.; Fletcher, S.; Katsonis, N. Conversion of Light into Macroscopic Helical Motion. *Nat. Chem.* **2014**, *6*, 229−235.
(21) Wang, Y.; Dang, A.; Zhang, Z.; Yin, R.; Gao, Y.; Feng, L.; Yang, S. Repeatable and Reprogrammable Shape Morpging from Photo-responsvie Gold Nanorod/Liquid Crystal Elastomers. *Adv. Mater.* **2020**, *32*, No. 2004270.
(22) Cheng, Z.; Wang, T.; Li, X.; Zhang, Y.; Yu, H. NIR-Vis-UV Light-Responsive Actuator Films of Polymer-Dispersed Liquid Crystal/Graphene Oxide Nanocomposites. *ACS Appl. Mater. Interfaces* **2015**, *7*, 27494−27501.
(23) Ge, F.; Yang, R.; Tong, X.; Camerel, F.; Zhao, Y. A Multifunctional Dye-Doped Liquid Crystal Polymer Actuator: Light-Guided Transportation, Turning in Locomotion, and Autonomous Motion. *Angew. Chem. Inter. Ed.* **2018**, *57*, 11758−11763.
(24) Lan, R.; Sun, J.; Shen, C.; Huang, R.; Zhang, Z.; Zhang, L.; Wang, L.; Yang, H. Near-Infrared Photodriven Self-sustained Oscillation of Liquid Crystalline Network Film with Predesignated Polydopamine Coating. *Adv. Mater.* **2020**, *32*, No. 1906319.
(25) Shen, C.; Lan, R.; Huang, R.; Zhang, Z.; Bao, J.; Zhang, L.; Yang, H. Photochemically an Photothermally Controllable Liquid Crystalline Network and Soft Walkers. *ACS Appl. Mater. Interfaces* **2021**, *13*, 3221−3227.
(26) Wang, J.; Yang, B.; Yu, M.; Yu, H. Light-Powered Self-sustained Oscillators of Graphene Oxide/Liquid Cyrtsalline Network Composites Showing Amplitude and Frequency Superposition. *ACS Appl. Mater. Interfaces* **2022**, *14*, 15632−15640.
(27) Hu, Z.; Li, Y.; Lv, J. Phototunable Self-Osillating System Driven by a Self-Winding Fiber Actuator. *Nat. Commun.* **2021**, *12*, 3211.
(28) Chen, L.; Dong, Y.; Tang, C.; Zhong, L.; Law, W.; Tsui, G.; Yang, Y.; Xie, X. Development of Direct-Laser-Printable Light-Powered Nanocomposites. *ACS Appl. Mater. Interfaces* **2019**, *11*, 19541−19553.
(29) Lu, X.; Ambulo, C.; Wang, S.; Rivera-Tarazona, L.; Kim, H.; Searles, K.; Ware, T. 4D-Printing of Photoswitchable Actuators. *Angew. Chem., Int. Ed.* **2021**, *60*, 5536−5543.
(30) Cheng, Y.; Lu, H.; Lee, X.; Zeng, H.; Priimagi, A. Kirigami-Based Light-Induced Shape-Morphing and Locomotion. *Adv. Mater.* **2020**, *32*, No. 1906233.
(31) Hu, J.; Nie, Z.; Wang, M.; Liu, Z.; Huang, S.; Yang, H. Springtail-Inspired Light-Driven Soft Jumping Robots Based on Liquid Cyrtsal Elastomers with Monolithic Three-Leaf Panel Fold Structure. *Angew. Chem., Int. Ed.* **2023**, *62*, No. e202218227.
(32) Li, C.; Huang, X.; Jiang, H. Direct Sun-Driven Artificial Heliotropism Solar Energy Harvesting Based on a Photo-Thermo-mechanical Liquid Crystal Elastomer Nanocompsite. *Adv. Funct. Mater.* **2012**, *22*, 5166.
(33) Nie, Z.; Zuo, B.; Wang, M.; Huang, S.; Chen, X.; Liu, Z.; Yang, H. Light-Driven Continuous Rotating Möbius Strip Actuators. *Nat. Commun.* **2021**, *12*, 2334.
(34) Wang, J.; Zhao, T.; Fan, Y.; Wu, H.; Lv, J. Leveraging Bioinspired Structural Constraints for Tunable and Programmable Snapping Dynamics in High-Speed Soft Actuators. *Adv. Funct. Mater.* **2023**, *33*, No. 2209798.
(35) Zhang, Y.; Huang, L.; Song, H.; Ni, C.; Zhao, Q.; Xie, T. 4D Printing of a Digital Shape Memory Polymer with Tunable High Performance. *ACS Appl. Mater. Interfaces* **2019**, *11*, 32408−32413.
(36) Ni, C.; Xie, T. Spatio-temporal Programmable Supramolecular Shape Memory Polymer. *Acta Polym. Sin.* **2022**, *53*, 1161−1172.
(37) Xia, Y.; He, Y.; Zhang, F.; Liu, Y.; Leng, J. A Review of Shape Memory Polymers and Composites: Mechanisms, Materials, and Applications. *Adv. Mater.* **2021**, *33*, No. 2000713.
(38) Lendlein, A.; Gould, O. E. C. Reprogrammable Recovery and Actuation Behaviour of Shape-Memory Polymers. *Nat. Rev. Mater.* **2019**, *4*, 116−133.
(39) Zhang, X.; Zhu, C.; Xu, B.; Qin, L.; Wei, J.; Yu, Y. Rapid, Localized, and Athermal Shape Memory Performance Triggered by Photoswitchable Glass Transition Temperature. *ACS Appl. Mater. Interfaces* **2019**, *11*, 46212−46218.
(40) Huang, X.; Qin, L.; Wang, J.; Zhang, X.; Peng, B.; Yu, Y. Multiple Shape Manipulation of Liquid Crystal Polymers Containing Diel-Alder Network. *Adv. Funct. Mater.* **2022**, *32*, No. 2208312.
(41) Peng, W.; Zhang, G.; Liu, J.; Nie, S.; Wu, Y.; Deng, S.; Fang, G.; Zhou, J.; Song, J.; Qian, J.; Pan, P.; Zhao, Q.; Xie, T. Light-Coded Digital Crystallinity Patterns toward Bioinspired 4D Tansformation of Shape Memory Polymers. *Adv. Funct. Mater.* **2020**, *30*, No. 2000522.
(42) Wang, M.; Li, J.; Yang, H. Dynamic Diselenide Bond-Enabled Liquid Crystal Elastomer-based Two-Way Shape Memory Aerogels with Weldability and Closed-Loop Recyclability. *Smart Molecules* **2023**, *1*, No. e20230009.
(43) Fang, Z.; Zheng, N.; Zhao, Q.; Xie, T. Healable, Reconfigurable, Reprocessable Thermoset Shape Memory Polymer with Highly Tunable Topological Rearrangement Kinetics. *ACS Appl. Mater. Interfaces* **2017**, *9*, 22077−22082.
(44) Lendlein, A.; Jiang, H.; Juger, O.; Langer, R. Light-Induced Shape-Memory Polymers. *Nature* **2005**, *434*, 879−882.
(45) Jin, B.; Song, H.; Jiang, R.; Song, J.; Zhao, Q.; Xie, T. Programming a Crystalline Shape Memory Polymer Network with Thermo and Photo-Reversible Bonds Toward a Single-Component Soft Robot. *Sci. Adv.* **2018**, *4*, No. eaao3865.
(46) Zhu, C.; Li, C.; Wang, H.; Hong, W.; Huang, F.; Zheng, Q.; Wu, Z. Reconstructable Gradient Structures and Reprogrammable 3D Deformations of Hydrogels with Coumarin Units as the Photolabile Crosslinks. *Adv. Mater.* **2021**, *33*, No. 2008057.
(47) Wu, Y.; Hu, Z.; Huang, H.; Chen, Y. The Design of Triple Shape Memory Polymers with Stable yet Tunable Temporary Shapes by Introducing Photo-Responsive Units into a Crystalline Domain. *Poly. Chem.* **2019**, *10*, 1537−1543.
(48) Zhang, Y.; Ma, W.; Zhong, J.; Zhou, Z.; Yang, H.; Cao, Z.; Wang, S. Rapid Shape Recovery and Remodeling by Tuning the Topology of Polycaprolactone-Based Polymer Networks. *Polymer* **2024**, *292*, No. 126641.
(49) Kumar, K.; Knie, C.; Bleger, D.; Peletier, M.; Friedrich, H.; Hecht, S.; Broer, D.; Debije, M.; Schenning, A. A Chaotic Self-Oscollating Sunlight-Driveb Polymer Actuator. *Nat. Commun.* **2016**, *7*, 11975.
(50) Zeng, H.; Wani, O.; Wasylczyk, P.; Kaczmarek, R.; Priimagi, A. Self-Regualting Iris Based on Light-Actuated Liquid Crystal Elastomer. *Adv. Mater.* **2017**, *29*, No. 1701814.
(51) Gelebart, A.; Jan Mulder, D.; Varga, M.; Konya, A.; Vantomme, G.; Meijer, E.; Selinger, R.; Broer, D. Making Waves in a Photoactive Polymer Film. *Nature* **2017**, *546*, 632−636.
(52) Chen, Y.; Jean, C. Polyethers containing coumarin dimer components in the main chain. II. Reversible photocleavage and photopolymerization. *J. Appl. Polym. Sci.* **1997**, *64*, 1759.
(53) Ling, J.; Rong, M.; Zhang, M. Photo-stimulated self-healing polyurethane containing dihydroxyl coumarin derivatives. *Polymer* **2012**, *53*, 2691.
(54) Ling, J.; Rong, M.; Zhang, M. Coumarin imparts repeated photochemical remendability to polyurethane. *J. Mater. Chem.* **2011**, *21*, 18373.

https://doi.org/10.1021/acsami.5c12533
ACS Appl. Mater. Interfaces 2025, 17, 48815−48823